THE JOURNAL OF PHYSICAL CHEMISTRY C
A JOURNAL OF THE AMERICAN CHEMICAL SOCIETY

pubs.acs.org/JPCC
Article

Investigating Pb Nanostructures with a Density-Functional Tight-Binding Approach: Slater–Koster Parameters

Andres Unigarro, Florian Günther, and Sibylle Gemming*

Cite This: J. Phys. Chem. C 2025, 129, 5617–5624

ABSTRACT: Intercalation in epigraphene systems is an established technique widely used to modify the electronic structure of graphene and to synthesize otherwise unstable two-dimensional layers with exotic electronic properties. However, capturing the full symmetry of the heterostructure requires a large number of atoms, rendering traditional electronic-structure approaches computationally demanding. Density-functional-based tight-binding (DFTB) offers an efficient alternative, balancing accuracy and reduced computational cost. For heavy elements such as Pb, however, proper parameters for these types of calculations are not available in the open literature. In this work, we developed a Slater–Koster parameter set for the elements Si, C, and Pb, enabling the investigation of the electronic structure of various elemental and binary solid-state structures, such as graphene, plumbene, and silicon carbide. Our results obtained with DFTB for bulk Pb and Pb/SiC structures show good qualitative agreement with pure DFT calculations. Furthermore, the inclusion of spin–orbit coupling (SOC) significantly modifies their electronic properties, aligning with DFT findings. These results underscore the capability of the optimized parameters to accurately model complex systems, allowing investigations of larger systems closer to experimental observations.

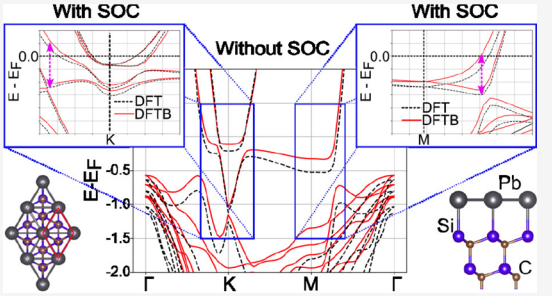

INTRODUCTION

Density functional theory (DFT)[1] within the Kohn–Sham formulation,[2] is a reliable method for investigating the electronic properties of molecules, clusters and condensed matter systems. Nowadays, efficient DFT-KS codes, coupled with high-performance computing systems, have led to the possibility of studying complex and large systems.[3] However, the complexity and size of the systems required for modern investigations are growing faster than the nominal compute power and the algorithmic optimization of DFT codes. For example, in systems such as epitaxial graphene grown on SiC(0001), the lattice mismatch between graphene and the SiC substrate leads to the formation of a nearly commensurate $(6\sqrt{3} \times 6\sqrt{3})R30°$ superstructure relative to the SiC(1×1) surface cell, as demonstrated in previous experiments.[4,5] Accurately modeling this system while preserving its full symmetry requires a supercell containing 1310 atoms,[6] which introduces significant computational challenges for realistic calculations. To study such heterostructures, a common approach is to simplify the problem by considering an approximate system that retains the essential features of the full system. For example, strain or compression is usually applied to one of the materials to achieve a better match between the lattice constants, thereby reducing the size of the system considered. Alternatively, to study those systems without altering their mechanical properties, approximate theoretical methods capable of accurately describing specific properties of interest (e.g., vibrational properties, electronic transport, etc.) without including all the interactions involved can be used. In that way, larger systems can be studied while reducing the computational demands.

One alternative to DFT is provided by classical force field methods (i.e., empirical potentials) which are several orders of magnitude faster, allowing the study of the dynamics of systems composed of up to millions of particles beyond the nanosecond regime. That method, however, requires the definition of numerous empirical parameters for a specific system. The availability of accurate parameters for a number of chemical elements can be limited, and their transferability between different bonding types and material systems may be low, which limits the application of such approaches. Furthermore, because force field methods ignore the electronic contributions,[7] they yield geometries of van der Waals stacked 2D materials well,[8,9] but they can not describe electron distributions, band structures including spin–orbit coupling (SOC), transport properties and interlayer bond and compound formation.

Received: October 29, 2024
Revised: February 14, 2025
Accepted: March 3, 2025
Published: March 11, 2025

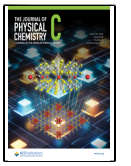

In order to address the scalability problem in solid-state physics, tight-binding (TB) methods were developed. In the 1980s Seifert and co-workers,[10] reported the use of a restricted atomic orbital (AO) basis set representation for an approximate treatment of Kohn−Sham DFT. In the subsequent years, these early ideas were further developed resulting in the so-called density-functional based tight binding scheme (DFTB).[11−14] As reported in the literature,[11,15−20] this method has been successfully applied to studying a variety of condensed matter systems with a broad range of elements and its implementation can be orders of magnitude faster than DFT. The computational efficiency of DFTB relies on the fact that the involved interactions are reduced to two center term only, allowing for a precalculation and tabulation of element-pair interactions employing the Slater-Koster (SK) method.[21] The parameters needed for the application of DFTB schemes, however, are not available for all atoms, e.g., Pb, Bi and Sn which have been widely used as intercalants in epigraphene systems.[22−26]

Here, we generate Slater-Koster parameters of the main group-IV elements: Si, C and Pb. These elements are formally isovalent, but exhibit very different electronic properties: the C 2*s* and 2*p* states from the sp^2 and sp^3 hybrid orbitals present in graphene and SiC, Si can further include the unoccupied 3*d* orbitals into bonding with intercalants, and the heavy element Pb features relativistic effects, which bind the 6*s* electrons more strongly to the atom core and lead to an addition splitting of the 6p shell. All these effects need to be accounted for when analyzing the observed multitude of intercalated epitaxial graphene systems. Since in this work we only focus on the electronic properties of the structures, our parametrization does not include interatomic potentials, i.e., the repulsive term, which would be necessary for the evaluation of geometries, forces, or phonons. The inclusion of the repulsive energy in the parametrization will be subject of a forthcoming work.

The work is structured as follows: First, a brief introduction to the main theoretical concepts utilized in DFTB, along with the principal equations of the method, is provided. Second, we discuss the results of a comparative investigation between the electronic structures obtained using our newly generated set of parameters and those results derived from DFT calculations, focusing on various elemental and binary solid-state structures, in particular graphene and silicon carbide. Given the primary emphasis of this work on the DFTB parametrization of Pb, we also examine bulk Pb as well as Pb on SiC interface structures. In the case of the Pb/SiC system, we restrict our study to the Pb(1 × 1) phase, for which density functional theory calculations have suggested its stability,[27,28] and which has been recently reported to form in the early stages of the Pb intercalation process.[29]

THEORETICAL APPROACH

A detailed derivation of DFTB from density functional theory (DFT) has been presented in the literature.[11,18,30−32] Therefore, the theoretical fundamentals of DFTB will be only briefly reviewed in the current work. According to DFT,[33,34] the ground state total energy of a system composed by N nuclei located at the positions $\mathbf{r}$ can be expressed as a unique function of the electronic density ρ. Within the Kohn−Sham formulation,[2] the atomic orbitals ψ_i describe a system of noninteracting electrons that have the same electronic density $\rho(\mathbf{r})$ as the interacting system. Then, $\rho(\mathbf{r})$ can be expressed as follows:

$$\rho(\mathbf{r}) = \sum_{i}^{\mathrm{occ}} |\psi_i(\mathbf{r})|^2 \tag{1}$$

Using the previous definition, the total energy of the system in the ground state is given as

$$E_{\mathrm{DFT}}[\rho] = \sum_i \epsilon_i - E_{\mathrm{H}}[\rho(\mathbf{r})] - \int \rho(\mathbf{r}) V_{\mathrm{XC}}[\rho(\mathbf{r})] \mathrm{d}^3 r + E_{\mathrm{XC}}[\rho(\mathbf{r})] \tag{2}$$

where

$$E_{\mathrm{H}} = -\frac{e}{2} \int \mathrm{d}^3\mathbf{r} \int \mathrm{d}^3\mathbf{r}' \frac{\rho(\mathbf{r})\rho(\mathbf{r}')}{|\mathbf{r} - \mathbf{r}'|} \tag{3}$$

is the Hartree energy and accounts for the classical electrostatic interaction energy of the electronic density,[33,34] E_{XC} is the exchange-correlation energy[33,34] and $V_{\mathrm{XC}} = \frac{\delta E_{\mathrm{XC}}[\rho(\mathbf{r})]}{\delta\rho}$. The orbital energy ϵ_i is calculated by solving the single-particle equations:

$$\hat{h^{KS}}|\psi_i\rangle = (\hat{t} + V_{\mathrm{ext}} + V_{\mathrm{H}}[\rho(\mathbf{r})] + V_{\mathrm{XC}}[\rho(\mathbf{r})])|\psi_i\rangle = \epsilon_i|\psi_i\rangle \tag{4}$$

In the previous relation $V_{\mathrm{H}} = \frac{\delta E_{\mathrm{H}}[\rho(\mathbf{r})]}{\delta\rho}$ and $\hat{t}$ is the kinetic energy of the noninteracting system. Following Foulkes and Haydock,[32] any electronic density ρ can be expressed in terms of a reference density ρ_0 plus some fluctuation $\delta\rho$, i.e:

$$\rho(\mathbf{r}) = \rho_0(\mathbf{r}) + \delta\rho(\mathbf{r}) \tag{5}$$

Expanding $E_{\mathrm{XC}}[\rho_0 + \delta\rho]$ in a Taylor series up to the second-order term:

$$E_{\mathrm{XC}}[\rho_0 + \delta\rho] \approx E_{\mathrm{XC}}[\rho_0] + \int \left.\frac{\delta E_{\mathrm{XC}}}{\delta\rho}\right|_{\rho_0} \delta\rho \mathrm{d}^3\mathbf{r} + \int \left.\frac{\delta^2 E_{\mathrm{XC}}}{\delta\rho\delta\rho'}\right|_{\rho_0} \delta\rho\delta\rho' \mathrm{d}^3\mathbf{r}\mathrm{d}^3\mathbf{r}' \tag{6}$$

allows to rewrite the total energy as

$$E_{\mathrm{tot}} \approx E_{\mathrm{BS}}[\rho_0] + E_{\mathrm{2nd}}[\rho_0, (\delta\rho_0)^2] + E_{\mathrm{rep}}[\rho_0] \tag{7}$$

where:

$$\begin{aligned} E_{\mathrm{BS}} &= \sum_i \left\langle \psi_i \middle| -\frac{1}{2}\nabla^2 + V_{\mathrm{ext}} + V_{\mathrm{H}}[\rho_0] + V_{\mathrm{XC}}[\rho_0] \middle| \psi_i \right\rangle \\ E_{\mathrm{2nd}} &= \frac{1}{2} \int\int \left(\left.\frac{\delta^2 E_{\mathrm{XC}}}{\delta\rho\delta\rho'}\right|_{\rho_0} + \frac{1}{|\mathbf{r} - \mathbf{r}|} \right) \delta\rho\delta\rho' \mathrm{d}^3 r \mathrm{d}^3 r' \\ E_{\mathrm{rep}} &= -E_{\mathrm{H}}[\rho_0] + E_{\mathrm{XC}}[\rho_0] - \int v_{\mathrm{XC}}[\rho_0]\rho_0 \mathrm{d}^3 r + E_{\mathrm{II}} \end{aligned} \tag{8}$$

In the DFTB scheme, the effective potential of the Kohn−Sham formulation is expressed as a superposition of spherical, atom-centered contributions associated with the atomic densities ρ^a, i.e., $V_{\mathrm{eff}}^{\mathrm{KS}}[\rho_0] = V_{\mathrm{ext}}[\rho_0] + V_{\mathrm{H}}[\rho_0] + V_{\mathrm{XC}}[\rho_0] \approx \sum_a V^a[\rho^a]$. This decomposition is possible for V_{ext} and V_{H} since they depend explicitly on ρ^a. For V_{XC}, however, this case represents an approximation due to its nonlinearity. In DFTB the KS orbitals ψ_i are expanded in terms of a linear combination of atomic orbitals (LCAO) ϕ_ν which are restricted to the valence shell of the atoms, namely, $\psi_i = \sum_\mu c_{\mu i}\phi_\mu$.[31]

https://doi.org/10.1021/acs.jpcc.4c07351
J. Phys. Chem. C 2025, 129, 5617−5624

Table 1. Confinement Radii are Given in Bohr, whereas Onsite Energies ϵ are Given in Hartree

element	valence shell	r_0^d	r_0^w	ϵ_d	ϵ_p	ϵ_s
C	$2s^2 2p^2$	9	3		−0.19436081	−0.50490762
Si	$3s^2\ 3p^2\ 3d^0$	7	5.4 5.4 3.3	0.02808580	−0.15061948	−0.39616322
Pb	$6s^2\ 6p^2\ 6d^0$	9	5	0.00529963	−0.14379385	−0.46859817

When only E_{BS} is considered, the secular equation that has to be solved is given by

$$\sum_{\nu} c_{\nu i}(H_{\mu\nu}^{BS} - \varepsilon_i S_{\mu\nu}) = 0 \text{ with } \nu \in b \text{ and } \mu \in a, \forall\ a, b \tag{9}$$

with the Hamiltonian matrix elements and the overlap matrix elements given by $H_{\mu\nu}^{BS} = \left\langle \phi_\mu^a | \hat{H}^0 | \phi_\nu^b \right\rangle$ and $S_{\mu\nu} = \langle \phi_\mu^a | \phi_\nu^b \rangle$ respectively. Neglecting three-center and crystal-field terms as well as pseudopotential contributions,[31] only two center terms remain in the Hamiltonian $H_{\mu\nu}^{BS}$. Therefore, in this representation the Hamiltonian matrix for DFTB is found as

$$H_{\mu\nu}^{BS} = \begin{cases} \varepsilon^{atom} & ,\mu = \nu \\ \left\langle \phi_\mu^a \middle| \hat{t} + V[\rho^a + \rho^b] \middle| \phi_\nu^b \right\rangle & ,\mu \neq \nu, \forall\ a \neq b \\ 0 & ,\text{else} \end{cases} \tag{10}$$

where ε^{atom} are the orbital energies of the isolated atoms and $V[\rho^a + \rho^b]$ the KS potentials of the superimposed atomic densities of the neutral atoms. It is worth mentioning that the superposition of the potentials of isolated atoms, rather than the superposition of densities, can also be employed to calculate the matrix elements of this Hamiltonian.[35] In order to account for a possible charge exchange in the system, charge fluctuations $\delta\rho^a$ terms must be included, i.e., E_{2nd} has to be taken into account. Using the Mulliken definition of atomic point charges[36] the Hamiltonian can be expressed as (for more details see refs 13 and 30):

$$H_{\mu\nu}^{SCC-DFTB} = H_{\mu\nu}^0 + \frac{1}{2} S_{\mu\nu} \sum_{a,b} \gamma_{ab} \Delta q_a \Delta q_b \tag{11}$$

Here, Δq_a is the charge of the atom a described by the corresponding charge fluctuation $\delta\rho^a$ and the matrix γ_{ab} which accounts for Coulombic and exchange-correlation interactions of the transferred charge. Since Δq depends on the basis coefficients, the eigenvalue problem in eq 9, must be solved self-consistently. The main advantage in relation to full DFT calculations is that the self-consistency in DFTB must be achieved for the charges Δq_a instead of the charge density ρ. For the calculation of the total energy of the system and structural optimizations, repulsive energies (E_{rep}) must be considered. Although it is possible to access these repulsive terms directly, in practice they are fitted to full DFT calculations.[11,30,37]

As mentioned above, in DFTB only valence electrons are considered in the LCAO, which are typically bound and localized around atoms in solids and molecules. Since atomic orbitals (AO) based on free atoms will be too diffuse for this purpose,[30] the KS equations are usually solved applying an additional confinement potential $\left(\frac{r}{r_0}\right)^n$ where typically $n = 2$.[38] Therefore, by solving:

$$\left[\hat{t} + V^a + \left(\frac{r}{r_0}\right)^2\right] |\phi_i\rangle = \tilde{\epsilon} |\phi_i\rangle \tag{12}$$

an optimized set of AOs with a faster radial decay is calculated. These orbitals are commonly defined to represent the so-called pseudoatom. In practice, different radii r_0 are used to determine the atomic orbitals and the atomic densities. First, DFT calculations are carried out using a density confinement radius r_0^d. At a second stage, DFT calculations are performed again using a wave functions compression radius r_0^w using the potentials and the density calculated at the first stage. Usually, the values of r_0^d and r_0^w are empirically determined. In the DFTB scheme, therefore, two parameters per element have to be determined at this stage, a confinement radius for the AO basis, and a confinement radius for the initial density. Once the AOs and the initial density are defined, the eq 9 can be solved. Note that as $H_{\mu\nu}^{BS}$ and $S_{\mu\nu}$ depend on two-center integrals only, they can be calculated and tabulated in advance as a function of the distance between atomic pairs. The calculated Hamiltonian matrix as well as the overlap matrix are usually stored in Slater-Koster tables.[21] Therefore, it is not necessary to recalculate any integral during a DFTB calculation.

COMPUTATIONAL DETAILS

The optimization of the initial structures as well as the reference band structure calculations were performed using density functional theory (DFT) as implemented in the ABINIT package.[39] As in this work heavy atoms such as Pb were employed, fully relativistic norm-conserving pseudopotentials with the generalized gradient approximation (GGA) in the Perdew−Burke−Ernzerhof (PBE)[40] formulation were used to evaluate the exchange-correlation potential. The structural relaxations were performed using a k-point grid of 8 × 8 × 1 and 8 × 8 × 8 for the bulk structures until residual forces smaller than 0.0025 eV/Å were achieved. For an accurate ground state energy a 12 × 12 × 1 grid (12 × 12 × 12 grid for the bulk structures) was adopted. In all cases, self-consistent calculations were performed using 2.7×10^{-8} eV as threshold for the convergence of the total energy and a cutoff energy of 1088 eV for the plane wave basis. The semiempirical density functional-based tight binding (DFTB) approach was used in its self-consistent extension[31] as implemented in the DFTB+ code.[41] The Slater-Koster parametrization was developed using the skgen routine incorporated in the skprogs package.

In the present work, we focus on the elements C, Si, and Pb and intercalated epitaxial graphene systems. Therefore, the confinement radii were chosen to achieve a good qualitative agreement with DFT regarding the electronic properties for graphene, bulk Pb, SiC and Pb/SiC structures. In all Pb/SiC structures, dangling bonds at the lower SiC surface were passivated with H atoms and a vacuum layer of 15 Å was considered in order to avoid spurious interactions with periodic images. To be consistent with the DFT calculations, the PBE[40] functional was employed for the generation of the

https://doi.org/10.1021/acs.jpcc.4c07351
J. Phys. Chem. C 2025, 129, 5617−5624

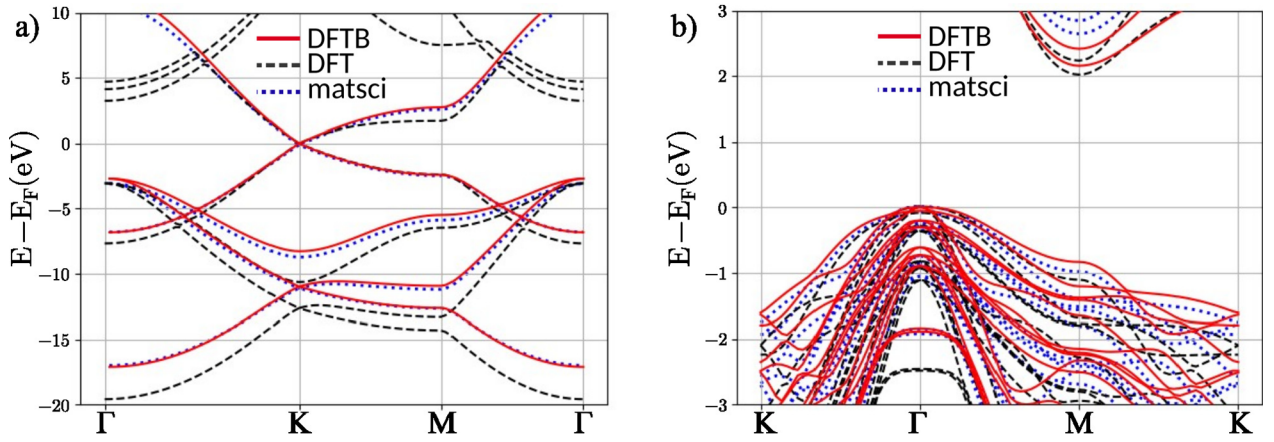

Figure 1. Band structures obtained with our DFTB parameters (red solid line), matsci-0-3 data set (blue dotted line), and DFT (black dashed line) for (a) graphene and (b) bulk 6H-SiC.

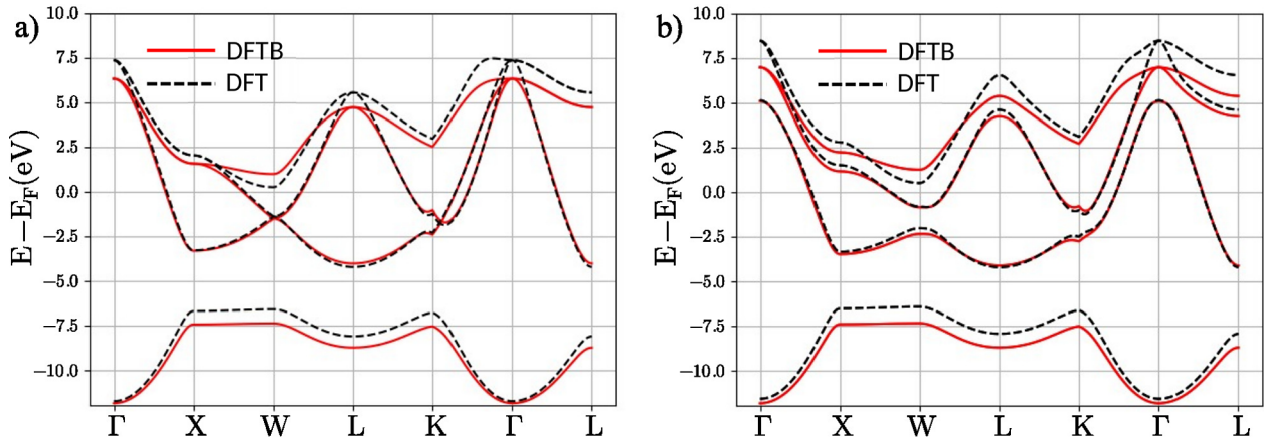

Figure 2. Band structures of bulk Pb (a) with and (b) without SOC calculated with our DFTB parameters (red solid line) and DFT (black dashed line).

DFTB parameters. The values used for the calculation of the SK tables are presented in Table 1 as well as the onsite energies obtained for each orbital. The onsite energies are found to be in accordance with values reported in the literature.[42] The set of SK tables generated in this work can be found as Supporting Information. For the band structure calculation, the maximum angular momentum was specified as p, d, p, and s for C, Si, Pb and H atoms, respectively. Note that since repulsive potentials were not included in our parametrization, the SK tables are not intended to be used to calculate geometrical properties of the systems. For this reason, the atomic structures used in the DFTB calculations were the same as those used to obtain the DFT results. The inclusion of such potentials is beyond the scope of this work.

RESULTS AND DISCUSSION

We begin our comparative study presenting the band structures of graphene and bulk 6H-SiC. For this purpose, we use as a reference the results calculated with DFT and DFTB, employing the semirelativistic Slater-Koster tables for material science simulation (matsci-0-3).[43] For graphene, the optimum DFT lattice constant of 2.46 Å was used. From Figure 1a it is possible to observe a good qualitative agreement with DFT calculations, especially around the Fermi level. Some deviations are expected given the minimal basis approximation in DFTB, and some compression of the bands toward the Fermi level can be noticed. In the case of SiC (see Figure 1b), the lattice constants used were $a = b = 3.08$ Å and $c = 15.2$ Å. Overall, a good qualitative agreement between the theoretical methods can be observed and band gap values of 2, 2.1 and 2.6 eV for DFT, DFTB and DFTB-matsci, respectively, are obtained. The difference in the band gap value obtained with the DFTB-matsci parametrization may be related to the fact that these parameters were calculated using LDA[44] functional. On the other hand, as the DFT calculations as well as the generation of the DFTB parameters were developed using the PBE functional, a underestimation of the band gap by about 1 eV it is expected, as this is a well-known feature of this functional.[45]

We proceed to evaluate the DFTB parameters generated for the Pb atom. For this purpose we consider the bulk phase of Pb which has a face-centered-cubic (fcc) crystal structure and a lattice constant $a_{Pb} = 4.95$ Å.[46] From Figure 2 it is possible to observe the good qualitative agreement between the band structures obtained with DFT and DFTB along some of the high-symmetry points of the first Brillouin zone (BZ). It is expected that the electronic properties of heavy atoms such as Pb may be affected by the spin−orbit coupling (SOC).[47,48] Therefore, the simulation of the band structure was carried out without (Figure 2a) and with (Figure 2b) the inclusion of the spin−orbit interaction. The results obtained in the present work are in accordance with other theoretical calculations

https://doi.org/10.1021/acs.jpcc.4c07351
J. Phys. Chem. C 2025, 129, 5617−5624

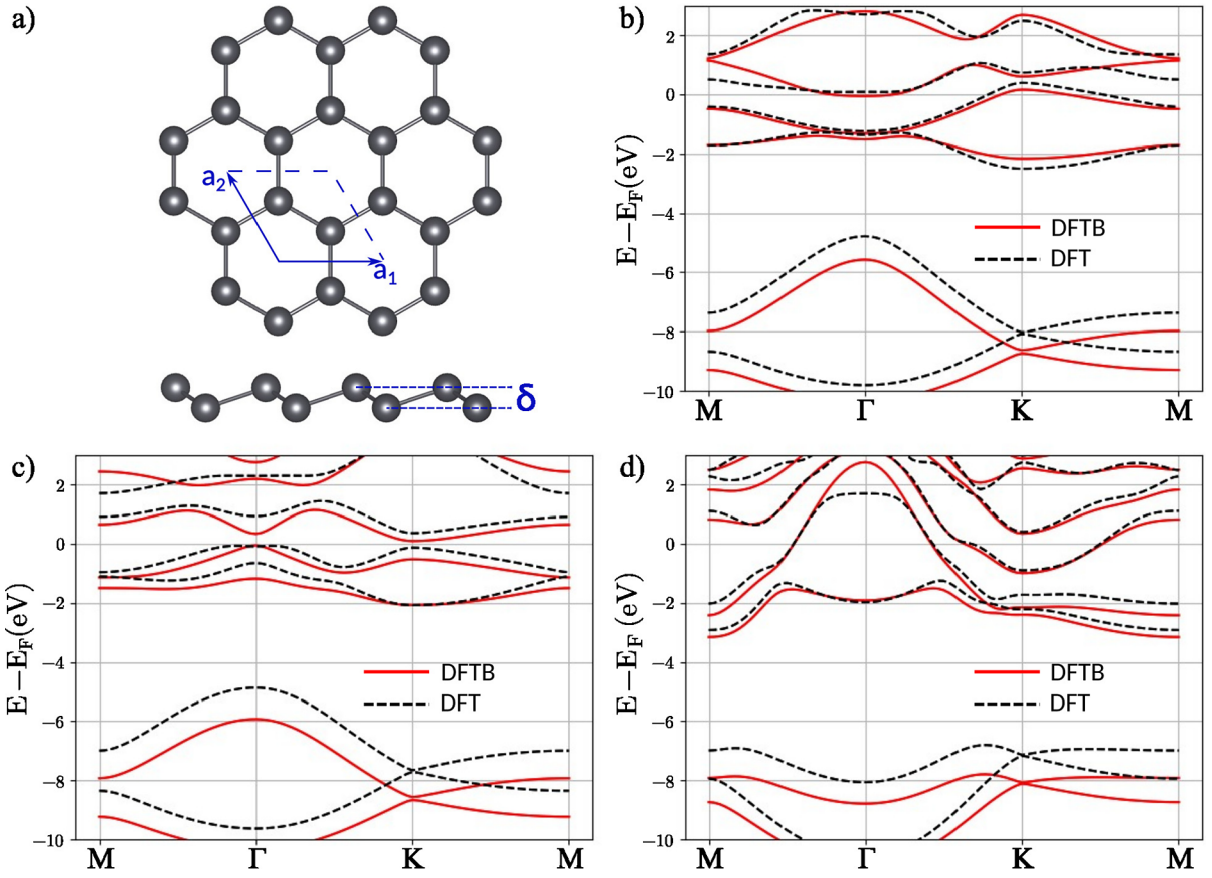

Figure 3. (a) Lattice structure of plumbene. Band structures obtained with DFTB (red solid line) and DFT (black dashed line) for (b) planar, (c) low-buckled, and (d) high-buckled plumbene, including spin−orbit interaction.

reported in the literature.[47,49] As depicted in Figure 2, the bands affected due to the SOC are mainly those which have p-orbital character (see Figure S1). The inclusion of the SOC, however, has little impact on the states close to the Fermi level. The most notable changes due to the SOC are observed along the symmetry directions $\Gamma - X$, $\Gamma - L$ and $K - \Gamma$ where the band splitting at the symmetry points Γ, W, and L obtained with DFTB (DFT) have the values 1.99 eV (3.33 eV), 1.49 eV (1.19 eV) and 1.13 eV (1.93 eV) respectively. We also observe that in the vicinity of the zone boundary point W and close to the K point in the $K - \Gamma$ direction, the SOC inclusion leads to the avoided band-crossings.

In order to complete our study on homoatomic Pb structures, we perform a DFT study on the structural, energetic and electronic properties of a 2D Pb layer with a potentially buckled honeycomb lattice structure (see Figure 3a) usually referred to as plumbene.[51,53] Unlike graphene, which features a planar honeycomb structure due to strong π-bonding, plumbene has two buckled structures that present lower energy than the planar configuration. As presented in Table 2, after DFT relaxations we obtain lattice constants of 5.23, 4.96, and 3.73 Å for the planar, low buckled (LB) and high buckled (HB) structures respectively, which are consistent with the values reported in the literature.[19,51,52] In general, out-of-plane buckling may exist depending on the relative stability of sp^2 and sp^3 hybridization as well as the exchange-correlation potential.[54] Similar to Si and Ge 2D structures, in plumbene, there exists a significant interelectron (lattice) repulsive Coulomb potential.[54] To reduce this repulsion, atoms are shifted relative to each other in the out-of-plane direction, leading to a weak $\pi - \pi$ overlap and a reduction in the bond length. The p_z orbitals, therefore, overlap more effectively with the s orbitals, which cause a mixed sp^2/sp^3 hybridization of electron states. As observed from previous results, the bonding character approaches sp^3 for heavier atoms,[55] making the sp^2 hybridization less favorable for Pb. The buckling has important consequences for the physical properties of the structure. On the one hand, mixed sp^2/sp^3 hybridization and the tendency to form sp^3 bonds make them more chemically active.[55] On the other hand, the point group symmetry of the lattices is reduced from D_{6h} to D_{3d} when transitioning from the planar to the buckled structure, which modifies the electronic properties of the material.

Table 2. Energetic and Structural Parameters Obtained after DFT Relaxations[a]

structure	$\lvert\Delta E\rvert$ (eV)	lattice constant (Å)	buckling (Å)
planar	1.00	5.38[50]; 5.23	0.0
low buckled	0.62	4.92[51]; 4.93[50]; 4.96	0.94[51]; 0.98
high buckled	0.00	3.57[52]; 3.69[50]; 3.73	2.55[50]; 2.55

[a]The total energy difference ΔE is defined as the energy of a structure minus the energy of the most stable structure, in this case the HB.

In Figure 3b−d, the band structures obtained using DFT and DFTB considering SOC are presented (for the band structures without SOC see Figure S2). In all three cases, both methods exhibit good qualitative agreement, especially around the Fermi energy. The results indicate that while the planar and HB structures exhibit metallic properties, the LB structure is a semiconductor with an indirect band gap of 0.5 eV (0.15

https://doi.org/10.1021/acs.jpcc.4c07351
J. Phys. Chem. C 2025, 129, 5617−5624

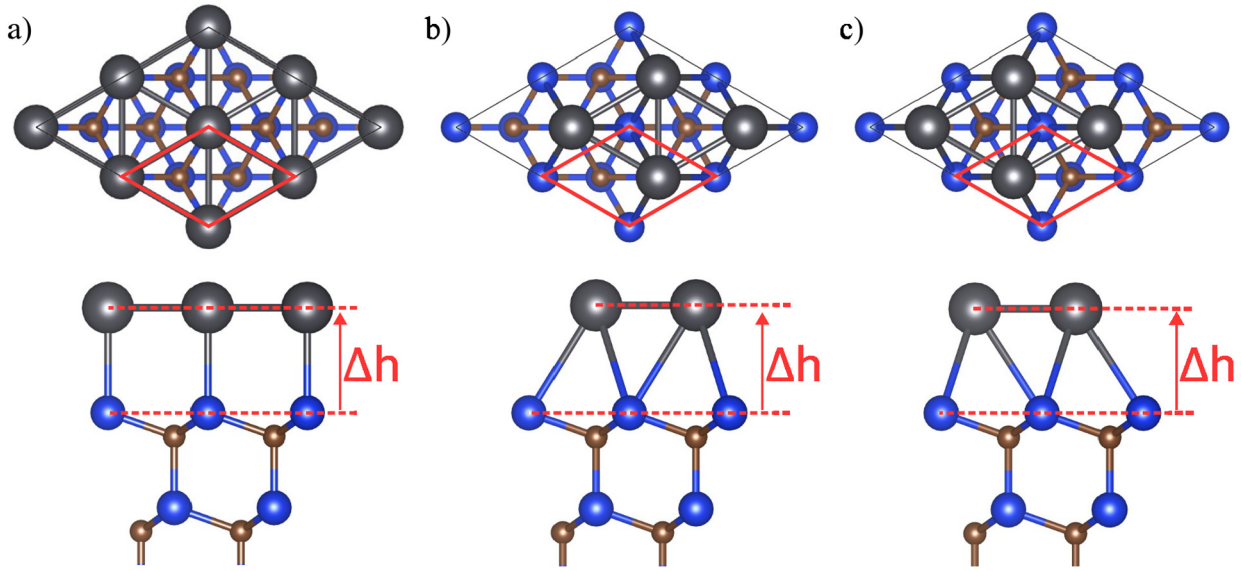

Figure 4. Atomic models of (1 × 1)-Pb/SiC(0001) for the three different absorption sites: (a) T1, (b) T4, and (c) H3.

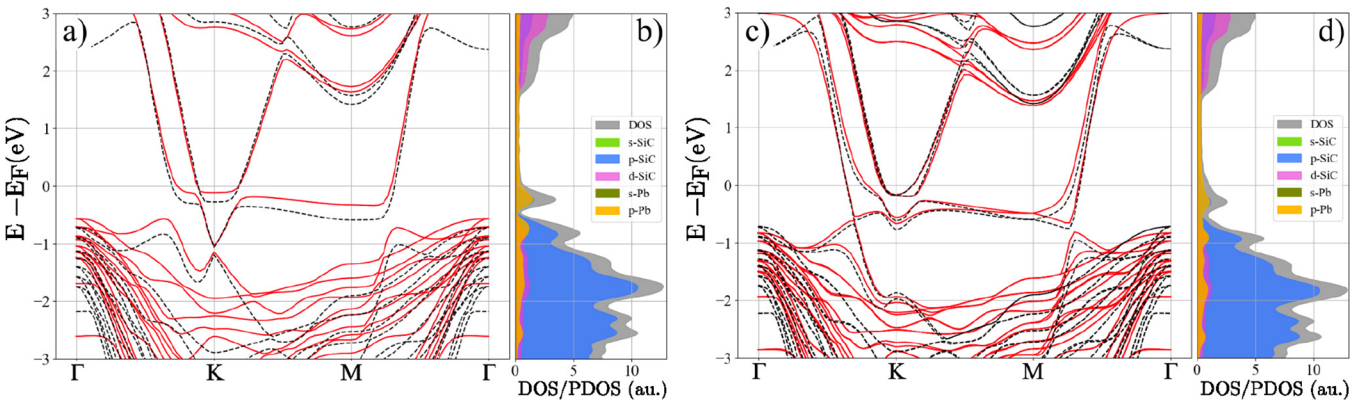

Figure 5. Comparison of the electronic band structure for the Pb/SiC system with Pb at the T1 position, obtained from DFT (black dashed line) and DFTB (red solid line). Panels (a) and (c) show the results without and with spin−orbit coupling (SOC), respectively. The figure also presents the density of states (DOS) and projected density of states (PDOS) obtained from DFTB (b) without and (d) with the inclusion of SOC.

eV) as obtained from DFT (DFTB). This band gap is larger than those reported in previous theoretical calculations for other group XIV elements, which are 10^{-3}, 8.23, and 72 meV for graphene, silicene, germanene, and stanene, respectively.[56] In the LB case when no SOC is considered, two bands cross linearly at the *K* point, showing Dirac-cone-like features (Figure S2b). Additionally, the valence band and conduction band touch at the Γ point. When SOC is included, however, the degeneracy is lifted and gaps open at both points. Similar to the results in plotted in Figures 1 and 2, a shift in the lower energy bands is observed in the DFTB results relative to the DFT results for all cases.

From the previously discussed results, we observed good qualitative agreement between DFT and DFTB calculations for graphene, SiC, and homoatomic Pb structures when considered individually. Now, in order to evaluate the performance of the full set of parameters, we focus our attention on the (1 × 1) phase of Pb on 6H-SiC, i.e., a uniform Pb layer with SiC-(1 × 1) periodicity. In this triangular lattice, the distance between Pb atoms is 3.08 Å. For the hexagonal SiC(0001) structure there exist three high-symmetry absorption sites on which the Pb atom can be located, namely, T1, H3, and T4 (see Figure 4). As presented in Figure S3 of the Supporting Information, the energy difference shows that the most stable structure is obtained when the Pb atom is located at the T1 site. After optimization, the values of Δ*z* (see Figure 4) obtained for T1, T4, and H3 positions were 2.81, 2.86, and 2.75 Å respectively.

Next, we analyze the band structure of the system with the lowest energy without and with SOC. The band structures obtained for the remaining models can be found in the SI. As shown in Figures 5a,c and S4, the band structures obtained from DFT and DFTB exhibit good qualitative agreement with and without SOC. When no SOC is included in the calculations, as it is evident from Figure 5a, a quasi-linear dispersion is observed around −1.2 eV below the Fermi level at *K* with a small gap of about 0.13 and 0.1 eV for DFT and DFTB results, respectively. This linear dispersion, mainly originates from p_x and p_y orbitals (see Figure S6). Interestingly, around the Fermi level a shallower dispersion can be identified, which as observed from the partial density of states (PDOS) obtained from DFTB (Figure 5b), arises from contributions of the *p* orbitals of both the Pb layer and the substrate, indicating a significant interaction between them. In order to investigate

https://doi.org/10.1021/acs.jpcc.4c07351
J. Phys. Chem. C 2025, 129, 5617−5624

further this interaction, the orbital-projected band structure of an artificial freestanding Pb(1 × 1) monolayer is calculated (Figure S5), from which a parabolic dispersion with p_z character it is observed around Γ. Upon interfacing with the SiC substrate (see Figure S6), the p_z orbitals hybridize with substrate dangling bonds, leading to the shallower dispersion observed near the Fermi level. When the SOC is included in the calculations, as displayed in Figure 5c, the bands at the *K* point split, causing the linear dispersion to disappear. Furthermore, the bands close to the Fermi level show a Rashba-like splitting around *K* and the flatter dispersion near the Fermi level in the direction $K - M$ can still be observed. Close to the *M* symmetry point in the $\Gamma - M$ direction, the band splitting of the band below the Fermi level takes the values of 0.42 and 0.5 eV for the band structures obtained with DFT and DFTB respectively. Also, from the PDOS (Figure 5b,d) and the orbital-projected band structure (see Figure S6) it is evident that in the range of 0 and 1.4 eV only *p*-type orbitals of Pb contribute to the electronic states in both with and without SOC cases.

CONCLUSIONS

A comparative study between DFT and DFTB using the new set of Slater-Koster parameters has been presented. It was found that our parameter set provides a good qualitative description for systems composed of C, Si, and Pb atoms. In the case of bulk Pb, significant impacts of spin−orbit coupling (SOC) were observed, particularly affecting the p-type bands around the Γ, *L*, and *M* symmetry points. Investigation into the three configurations of plumbene revealed that due to a substantial lattice Coulomb repulsive potential, the hexagonal Pb structure prefers to form buckled structures. Among these, the high buckled structure exhibited the lowest energy. Furthermore, while the planar and high buckled structures are metallic, the low buckled structure exhibits a band gap of 0.5 and 0.15 eV in DFT and DFTB, respectively. In order to evaluate the performance of the complete set of parameters, we examined a SiC(0001)-(1 × 1)-Pb system, where Pb can occupy three absorption positions: T1, T4, and H3. It was found that the most stable structure occurs when the Pb atom is positioned at T1. In the absence of SOC, a quasi-linear dispersion was observed around −1.2 eV below the Fermi level at the *K* point, with a small gap of approximately 0.13 and 0.1 eV in DFT and DFTB, respectively. Upon adding SOC, the bands split and the linear dispersion disappeared. Therefore, the spin−orbit interaction plays an important role in the system and strongly affects its electronic structure. Overall, our parameter set for DFTB calculations enables an accurate qualitative description of these systems. As DFTB is a computationally efficient method, this opens the possibility to investigate bigger systems closer to the structures observed experimentally.

ASSOCIATED CONTENT

Supporting Information

The Supporting Information is available free of charge at https://pubs.acs.org/doi/10.1021/acs.jpcc.4c07351.

Slater−Koster tables used in this manuscript (ZIP)

Supplementary results (PDF)

AUTHOR INFORMATION

Corresponding Author

Sibylle Gemming − *Technische Universität Chemnitz, Institut für Physik, 09107 Chemnitz, Germany;* orcid.org/0000-0003-0455-1945; Email: sibylle.gemming@physik.tu-chemnitz.de

Authors

Andres Unigarro − *Technische Universität Chemnitz, Institut für Physik, 09107 Chemnitz, Germany;* orcid.org/0009-0002-3283-5283

Florian Günther − *Departamento de Física, Universidade Estadual Paulista, Instituto de Geociências e Ciências Exatas, Rio Claro 13506-900, Brazil;* orcid.org/0000-0001-5002-4172

Complete contact information is available at: https://pubs.acs.org/10.1021/acs.jpcc.4c07351

Notes

The authors declare no competing financial interest.

ACKNOWLEDGMENTS

The authors acknowledge funding from the Deutsche Forschungsgemeinschaft via FOR 5242, project T1 (449119662), and Fundação de Amparo à Pesquisa do Estado de São Paulo via 2024/07315-1.

REFERENCES

(1) Hohenberg, P.; Kohn, W. Density functional theory (DFT). *Phys. Rev.* **1964**, *136*, B864.

(2) Kohn, W.; Sham, L. J. Self-consistent equations including exchange and correlation effects. *Physical review* **1965**, *140*, A1133.

(3) Pakdel, S.; Rasmussen, A.; Taghizadeh, A.; Kruse, M.; Olsen, T.; Thygesen, K. S. High-throughput computational stacking reveals emergent properties in natural van der Waals bilayers. *Nat. Commun.* **2024**, *15*, 932.

(4) Ohta, T.; Bostwick, A.; Seyller, T.; Horn, K.; Rotenberg, E. Controlling the Electronic Structure of Bilayer Graphene. *Science* **2006**, *313*, 951−954.

(5) Forbeaux, I.; Themlin, J.-M.; Debever, J.-M. Heteroepitaxial graphite on 6H−SiC(0001): Interface formation through conduction-band electronic structure. *Phys. Rev. B* **1998**, *58*, 16396−16406.

(6) Cavallucci, T.; Tozzini, V. Multistable Rippling of Graphene on SiC: A Density Functional Theory Study. *J. Phys. Chem. C* **2016**, *120*, 7670−7677.

(7) Leach, A. R. *Molecular modelling: principles and applications*; Pearson Education, 2001.

(8) Naik, M. H.; Maity, I.; Maiti, P. K.; Jain, M. Kolmogorov−Crespi Potential For Multilayer Transition-Metal Dichalcogenides: Capturing Structural Transformations in Moiré Superlattices. *J. Phys. Chem. C* **2019**, *123*, 9770−9778.

(9) Liang, Q.; Jiang, W.; Liu, Y.; Ouyang, W. Anisotropic Interlayer Force Field for Two-Dimensional Hydrogenated Carbon Materials and Their Heterostructures. *J. Phys. Chem. C* **2023**, *127*, 18641−18651.

(10) Seifert, G.; Eschrig, H.; Bieger, W. An approximation variant of LCAO-X-ALPHA methods. *Z. Phys. Chem. Leipzig* **1986**, *267*, 529−539.

(11) Porezag, D.; Frauenheim, T.; Köhler, T.; Seifert, G.; Kaschner, R. Construction of tight-binding-like potentials on the basis of density-functional theory: Application to carbon. *Phys. Rev. B* **1995**, *51*, 12947.

(12) Seifert, G.; Porezag, D.; Frauenheim, T. Calculations of molecules, clusters, and solids with a simplified LCAO-DFT-LDA scheme. *International journal of quantum chemistry* **1996**, *58*, 185−192.

(13) Elstner, M.; Porezag, D.; Jungnickel, G.; Elsner, J.; Haugk, M.; Frauenheim, T.; Suhai, S.; Seifert, G. Self-consistent-charge density-functional tight-binding method for simulations of complex materials properties. *Phys. Rev. B* **1998**, *58*, 7260.
(14) Seifert, G. Tight-binding density functional theory: an approximate Kohn- Sham DFT scheme. *J. Phys. Chem. A* **2007**, *111*, 5609−5613.
(15) Fowler, P.; Heine, T.; Manolopoulos, D.; Mitchell, D.; Orlandi, G.; Schmidt, R.; Seifert, G.; Zerbetto, F. Energetics of fullerenes with four-membered rings. *J. Phys. Chem.* **1996**, *100*, 6984−6991.
(16) Ivanovskaya, V. V.; Ranjan, N.; Heine, T.; Merino, G.; Seifert, G. Molecular dynamics study of the mechanical and electronic properties of carbon nanotubes. *Small* **2005**, *1*, 399−402.
(17) Frauenheim, T.; Weich, F.; Köhler, T.; Uhlmann, S.; Porezag, D.; Seifert, G. Density-functional-based construction of transferable nonorthogonal tight-binding potentials for Si and SiH. *Phys. Rev. B* **1995**, *52*, 11492.
(18) Frauenheim, T.; Seifert, G.; Elstner, M.; Niehaus, T.; Köhler, C.; Amkreutz, M.; Sternberg, M.; Hajnal, Z.; Di Carlo, A.; Suhai, S. Atomistic simulations of complex materials: ground-state and excited-state properties. *J. Phys.: Condens. Matter* **2002**, *14*, 3015.
(19) Liu, H.; Elstner, M.; Kaxiras, E.; Frauenheim, T.; Hermans, J.; Yang, W. Quantum mechanics simulation of protein dynamics on long timescale. *Proteins: Struct., Funct., Bioinf.* **2001**, *44*, 484−489.
(20) Nair, M. N.; Palacio, I.; Celis, A.; Zobelli, A.; Gloter, A.; Kubsky, S.; Turmaud, J.-P.; Conrad, M.; Berger, C.; de Heer, W.; et al. Band gap opening induced by the structural periodicity in epitaxial graphene buffer layer. *Nano Lett.* **2017**, *17*, 2681−2689.
(21) Slater, J. C.; Koster, G. F. Simplified LCAO method for the periodic potential problem. *Physical review* **1954**, *94*, 1498.
(22) Yang, D.; Xia, Q.; Gao, H.; Dong, S.; Zhao, G.; Zeng, Y.; Ma, F.; Hu, T. Fabrication and mechanism of Pb-intercalated graphene on SiC. *Appl. Surf. Sci.* **2021**, *569*, No. 151012.
(23) Schädlich, P.; Ghosal, C.; Stettner, M.; Matta, B.; Wolff, S.; Schölzel, F.; Richter, P.; Hutter, M.; Haags, A.; Wenzel, S.; et al. Domain Boundary Formation Within an Intercalated Pb Monolayer Featuring Charge-Neutral Epitaxial Graphene. *Adv. Mater. Interfaces* **2023**, *10*, No. 2300471.
(24) Matta, B.; Rosenzweig, P.; Bolkenbaas, O.; Küster, K.; Starke, U. Momentum microscopy of Pb-intercalated graphene on SiC: Charge neutrality and electronic structure of interfacial Pb. *Physical Review Research* **2022**, *4*, No. 023250.
(25) Hsu, C.-H.; Ozolins, V.; Chuang, F.-C. First-principles study of Bi and Sb intercalated graphene on SiC(0001) substrate. *Surf. Sci.* **2013**, *616*, 149−154.
(26) Mamiyev, Z.; Tegenkamp, C. Sn intercalation into the BL/SiC(0001) interface: A detailed SPA-LEED investigation. *Surfaces and Interfaces* **2022**, *34*, No. 102304.
(27) Yang, K.; Wang, Y.; Liu, C.-X. Momentum-Space Spin Antivortex and Spin Transport in Monolayer Pb. *Phys. Rev. Lett.* **2022**, *128*, No. 166601.
(28) Visikovskiy, A.; Hayashi, S.; Kajiwara, T.; Komori, F.; Yaji, K.; Tanaka, S. Computational study of heavy group IV elements (Ge, Sn, Pb) triangular lattice atomic layers on SiC(0001) surface. *arXiv* **2018**.
(29) Schölzel, F.; Richter, P.; Unigarro, A. D. P.; Wolff, S.; Schwarz, H.; Schütze, A.; Rösch, N.; Gemming, S.; Seyller, T.; Schädlich, P. Large-Area Lead Monolayers under Cover: Intercalation, Doping, and Phase Transformation. *Small Struct.* **2025**, *6*, No. 2400338.
(30) Koskinen, P.; Mäkinen, V. Density-functional tight-binding for beginners. *Comput. Mater. Sci.* **2009**, *47*, 237−253.
(31) Elstner, M.; Seifert, G. Density functional tight binding. *Philosophical Transactions of the Royal Society A: Mathematical, Physical and Engineering Sciences* **2014**, *372*, 20120483.
(32) Foulkes, W. M. C.; Haydock, R. Tight-binding models and density-functional theory. *Phys. Rev. B* **1989**, *39*, 12520.
(33) Parr, R. G. Density functional theory. *Annu. Rev. Phys. Chem.* **1983**, *34*, 631−656.
(34) Fiolhais, C.; Nogueira, F.; Marques, M. A. *A primer in density functional theory*; Springer Science & Business Media, 2003; Vol. *620*.
(35) Oliveira, A. F.; Seifert, G.; Heine, T.; Duarte, H. A. Density-functional based tight-binding: an approximate DFT method. *J. Braz. Chem. Soc.* **2009**, *20*, 1193−1205.
(36) Mulliken, R. S. Electronic population analysis on LCAO−MO molecular wave functions. *I. The Journal of chemical physics* **1955**, *23*, 1833−1840.
(37) Panosetti, C.; Anniés, S. B.; Grosu, C.; Seidlmayer, S.; Scheurer, C. DFTB modeling of lithium-intercalated graphite with machine-learned repulsive potential. *J. Phys. Chem. A* **2021**, *125*, 691−699.
(38) Eschrig, H. *Optimized LCAO Method and the Electronic Structure of Extended Systems*; De Gruyter: Berlin, Boston, 1988.
(39) Gonze, X.; Amadon, B.; Anglade, P.-M.; Beuken, J.-M.; Bottin, F.; Boulanger, P.; Bruneval, F.; Caliste, D.; Caracas, R.; Côté, M.; et al. ABINIT: First-principles approach to material and nanosystem properties. *Comput. Phys. Commun.* **2009**, *180*, 2582−2615.
(40) Perdew, J. P.; Burke, K.; Ernzerhof, M. Generalized gradient approximation made simple. *Physical review letters* **1996**, *77*, 3865.
(41) Aradi, B.; Hourahine, B.; Frauenheim, T. DFTB+, a sparse matrix-based implementation of the DFTB method. *J. Phys. Chem. A* **2007**, *111*, 5678−5684.
(42) Wahiduzzaman, M.; Oliveira, A. F.; Philipsen, P.; Zhechkov, L.; Van Lenthe, E.; Witek, H. A.; Heine, T. DFTB parameters for the periodic table: Part 1, electronic structure. *J. Chem. Theory Comput.* **2013**, *9*, 4006−4017.
(43) Frenzel, J.; Oliveira, A.; Jardillier, N.; Heine, T.; Seifert, G. Semi-relativistic, self-consistent charge Slater-Koster tables for density-functional based tight-binding (DFTB) for materials science simulations. *Zeolites* **2004**, *2*, 7.
(44) Perdew, J. P.; Wang, Y. Accurate and simple analytic representation of the electron-gas correlation energy. *Phys. Rev. B* **1992**, *45*, 13244−13249.
(45) Wang, X.; Zhao, J.; Xu, Z.; Djurabekova, F.; Rommel, M.; Song, Y.; Fang, F. Density functional theory calculation of the properties of carbon vacancy defects in silicon carbide. *Nanotechnology and Precision Engineering (NPE)* **2020**, *3*, 211−217.
(46) Zubizarreta, X.; Silkin, V. M.; Chulkov, E. V. First-principles quasiparticle damping rates in bulk lead. *Phys. Rev. B* **2011**, *84*, No. 115144.
(47) Heid, R.; Bohnen, K.-P.; Sklyadneva, I. Y.; Chulkov, E. Effect of spin-orbit coupling on the electron-phonon interaction of the superconductors Pb and Tl. *Phys. Rev. B* **2010**, *81*, No. 174527.
(48) Sklyadneva, I. Y.; Heid, R.; Echenique, P. M.; Bohnen, K.-B.; Chulkov, E. V. Electron-phonon interaction in bulk Pb: Beyond the Fermi surface. *Phys. Rev. B* **2012**, *85*, No. 155115.
(49) Zubizarreta, X.; Silkin, V. M.; Chulkov, E. V. Ab initio study of low-energy collective electronic excitations in bulk Pb. *Phys. Rev. B* **2013**, *87*, No. 115112.
(50) Lu, Y.; Zhou, D.; Wang, T.; Yang, S. A.; Jiang, J. Topological properties of atomic lead film with honeycomb structure. *Sci. Rep.* **2016**, *6*, 21723.
(51) Farzaneh, S.; Rakheja, S. Spin splitting and spin Hall conductivity in buckled monolayers of group 14: First-principles calculations. *Phys. Rev. B* **2021**, *104*, No. 115205.
(52) Rivero, P.; Yan, J.-A.; Garcia-Suarez, V. M.; Ferrer, J.; Barraza-Lopez, S. Stability and properties of high-buckled two-dimensional tin and lead. *Phys. Rev. B* **2014**, *90*, No. 241408.
(53) Yuhara, J.; He, B.; Matsunami, N.; Nakatake, M.; Le Lay, G. Graphene's latest cousin: Plumbene epitaxial growth on a "nano WaterCube". *Adv. Mater.* **2019**, *31*, No. 1901017.
(54) Takeda, K.; Shiraishi, K. Theoretical possibility of stage corrugation in Si and Ge analogs of graphite. *Phys. Rev. B* **1994**, *50*, 14916.
(55) Krawiec, M. Functionalization of group-14 two-dimensional materials. *J. Phys.: Condens. Matter* **2018**, *30*, 233003.
(56) Yu, X.-L.; Huang, L.; Wu, J. From a normal insulator to a topological insulator in plumbene. *Phys. Rev. B* **2017**, *95*, No. 125113.

https://doi.org/10.1021/acs.jpcc.4c07351
J. Phys. Chem. C 2025, 129, 5617−5624